

On the shapes and spins of "rubble pile" asteroids

Alan W. Harris, Space Science Institute

Eugene G. Fahnestock, Univ. of Michigan

Petr Pravec, Ondrejov Observatory

Abstract

We examine the shape of a "rubble pile" asteroid as it slowly gains angular momentum by YORP torque, to the point where "landsliding" occurs. We find that it evolves to a "top" shape with constant angle of repose from the equator up to mid-latitude. A similar calculation for a non-spinning, extremely elongate rubble pile body suggests that it should collapse into the rough shape of a prolate ellipsoid of about 2.5:1 axis ratio. We also investigate the tidal effects of a binary system with a "top shape" primary spinning at near the critical limit for stability. We find that very close to the stability limit, the tide from the secondary can actually levitate loose debris from the surface and re-deposit it, in a process we call "tidal saltation", such that angular momentum is transferred from the primary spin to the satellite orbit, thus maintaining the equilibrium of near-critical spin as YORP continues to add angular momentum to the system.

1. Introduction

In the recent *Science* papers by Ostro et al. (2006) and Scheeres et al., (2006) the asteroid (66391) 1999 KW4, shown in the cover illustration, is remarkable in having an almost constant surface slope, in the range of 30-35°, almost uniformly in the direction of the equator. The explanation appears to be that as 1999 KW4 is spun up by YORP, the local slope increases to the critical angle for land-sliding, which moves material toward the equator and re-establishes an equilibrium with the average slope of the surface being the angle of repose, which for most dry loose material is around 30-35°. The "top" shape appears to be the figure of quasi-equilibrium of a body that is spinning at a rate that is critical at the equator (gravity = centrifugal force), and has a constant slope at other latitudes, except for the poles, which would be pointed otherwise, and the equator, where slope must pass through zero. Indeed, the detailed shape of the figure allows us to infer the critical angle of slide of the regolith. In the first part of this paper we calculate the static figure of constant slope to compare with the radar-derived shape of 1999 KW4.

A second remarkable feature of 1999 KW4 is the extremely regular equatorial band, which is within about 1% of cancellation of gravity by centrifugal force. We suggest that this equilibrium is established by tidal forces from the satellite moving regolith around the equator. In the second part of this paper, we develop the equations of motion for material near the equator in the rotating frame of the primary, including tidal force from the secondary and sliding friction as material starts to move. We present numerical integrations of such mass motion to show that it results in a sort of "tidal torque" between the primary spin and the satellite orbit that transfers angular momentum to the satellite orbit, potentially much more rapidly than solid-body tides.

We are motivated in these studies by the fact that (66391) 1999 KW4 is not unique in these characteristics, indeed, it seems to be the archetypical case of an asynchronous binary system.

Many of the systems observed are found to have primaries with very low amplitude lightcurves (e.g., Pravec et al. 2006), indicating nearly circular equatorial profiles, and with spin periods very near the critical limit (Pravec and Harris 2007). Radar observations of a number of NEA asynchronous binary systems likewise indicate primaries with very regular equatorial profiles and spins near the critical limit (e.g., Shepard *et al.* 2006).

2. Constant-slope shape of a critically spinning body

The equilibrium figures of uniformly rotating fluids has been well studied (e.g., Chandrasekhar 1969). Up to a certain critical spin rate, the equilibrium figure of a homogeneous fluid is an oblate spheroid, a so-called Maclauren spheroid. At higher spin rates, an equilibrium triaxial ellipsoid figure exists, called Jacobi ellipsoids, up to a point where there is no equilibrium figure that can contain more angular momentum, and a body with still more angular momentum must fission in some manner to become a binary. These shapes are hardly relevant for small solid asteroids, even ones that are "rubble piles", with no tensile strength. The reason is that even strengthless rubble can sustain a slope against the pull of gravity, just as a sand pile does not flow like water but rather relaxes into a conical form with a rather constant slope, typically in the range of 35° or so. Thus we expect that the figure of a spinning asteroid can deviate from equilibrium (zero slope) by up to some critical angle before slumping (landsliding) occurs.

A brief digression into the subject of soil mechanics is in order. Geologists define two angles relating to the slope of rubble or other loose material. These angles are related to the coefficients of sliding (kinetic) friction and of static friction for the material. The condition for stability against landsliding is the maximum slope that a material such as sand, loose rock, or whatever can withstand before landsliding occurs. This angle is called the *angle of slide*, related to the coefficient of static friction: $\tan \beta_s = \mu_s$. A similar angle, the *angle of repose*, β_r , is the slope at which a landslide stops, or comes to rest. This angle is related to the coefficient of sliding (kinetic) friction: $\tan \beta_r = \mu_k$. The coefficient of sliding friction is always less than the coefficient of static friction (traction decreases once sliding starts, as a person driving in a skid discovers). For typical dry rubble on the Earth, the angle of repose is in the range of about 35° . The angle of slide is typically 5° to 10° greater. Thus nominal values $\beta_r = 35^\circ$ and $\beta_s = 42^\circ$ correspond to $\mu_k = 0.7$ and $\mu_s = 0.9$.

To model the quasi-equilibrium shape of a rubble pile, we first define a relation between the gravitational acceleration at the equator, g , and the centrifugal force due to rotational spin:

$$\omega^2 R = (1 - \delta)g = (1 - \delta)\omega_0^2 R, \quad (1)$$

where ω is the angular frequency of rotation and R is the equatorial radius of the body. ω_0 is the critical spin frequency at which acceleration is zero; for a sphere, $\omega_0^2 = GM / R^3$, but for a non-spherical body, it will differ a bit due to gravitational harmonics. The parameter δ is chosen such that the net acceleration at the equator is δ times the gravitational acceleration, and for $\delta = 0$ acceleration vanishes. In terms of spin rate, $\delta = 1 - (\omega / \omega_0)^2$, or $\omega / \omega_0 = \sqrt{1 - \delta}$. It is instructive to consider the local slope versus latitude for a sphere for various values of δ . This can be

computed analytically, which we have done in Figure 1. At the critical spin rate, local slope is just equal to the co-latitude. Note that slope begins to exceed a critical value of around 40° at a value of $\delta \approx 0.2$, which translates to a spin rate of $\omega/\omega_0 \approx 0.9$. Thus, we expect that an initially spherical "rubble pile" with a typical angle of repose would begin to experience landsliding as it were gradually spun up upon reaching about 90% of the critical spin rate ω_0 . This is consistent with the calculations of Holsapple (2004). However, in the

last 10% of spin-up, slopes reach extreme values, thus we expect slumping to occur. The onset should be in the mid-latitude range, around 20° - 30° , and with increasing spin should progress all the way to the equator quite rapidly. Note that "downhill" is always toward the equator, so slumping will only occur at latitudes less than where slope exceeds the critical value.

In order to compute quasi-equilibrium figures of a spinning body, we wrote a fairly simple program to numerically evaluate the gravity acceleration vector at the surface of a longitudinally symmetric body. We start with an oblate ellipsoid with flattening $f = c/a$ in the polar dimension, where c is the polar dimension and a is the equatorial dimension. We break the body up into cubic cells of $1/50$ the equatorial dimension, thus for a sphere, we have a little over half a million mass elements. We compute the acceleration of gravity at each degree of latitude on the body by adding up the acceleration from each of the individual "cubes" of mass. We then compute local slopes, for a set value of delta. We proceed iteratively, modifying the slope at any latitude where the value exceeds the critical value to a lower value in the direction of the equilibrium, and then we integrate the slopes starting from the equator to determine a new shape profile. Since the acceleration of gravity changes with shape, we must iterate several times to obtain convergence to a shape with constant

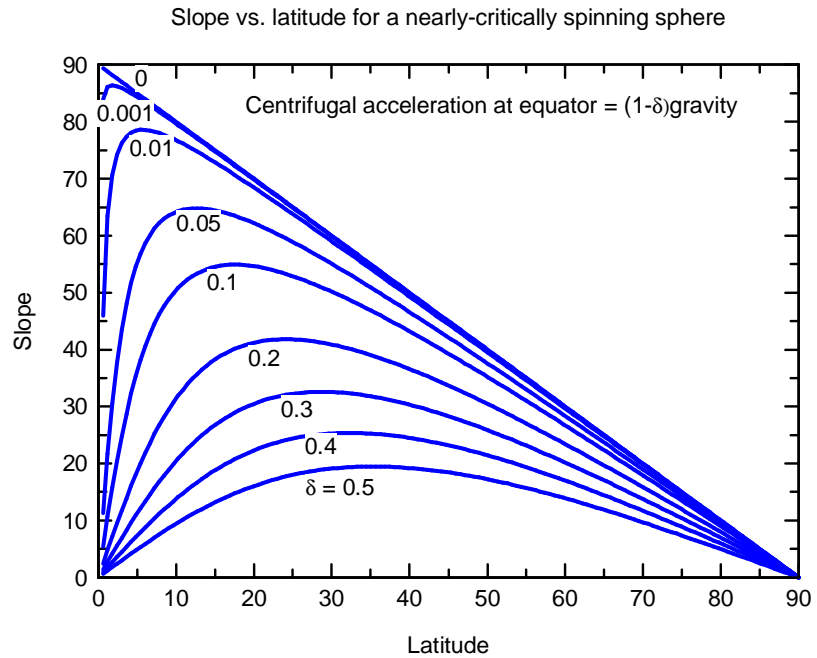


Figure 1. Slope vs. latitude for various values of δ

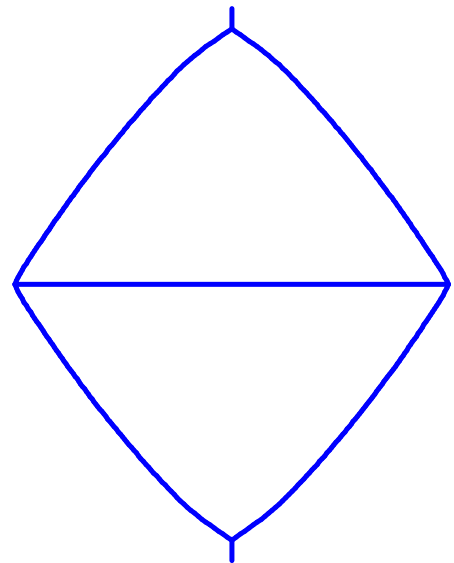


Figure 2. Shape with constant slope $\beta = 35^\circ$ at all latitudes, and equatorial acceleration $\delta = 0.01$.

slope. Our first test of the program was to specify a critical slope of zero corresponding to a fluid body, which should result in a Maclauren ellipsoid. We confirmed that we did get this result, and we verified the flattening of the computed ellipsoid at our chosen value of δ with that given by Chandrasekhar (1969) for an analytically computed Maclauren ellipsoid. For our first real calculation, we started from a sphere, chose a critical slope $\beta = 35^\circ$, and assumed a value of $\delta = 0.01$. We chose a non-zero value of δ in order to avoid the singularity of surface acceleration going completely to zero at the equator. The program converged on the shape shown in Figure 2. This shape is not too realistic, for one thing it has a greater moment of inertia about an axis through the equator than through the pole, so the stable rotational spin state would be about an axis through the equator. More importantly, though, starting from a sphere, evolution to this shape would involve "landsliding" uphill at higher latitudes, since as can be seen in Figure 1, the slope in the initial spherical figure is less than β at latitudes greater than about the complement of β .

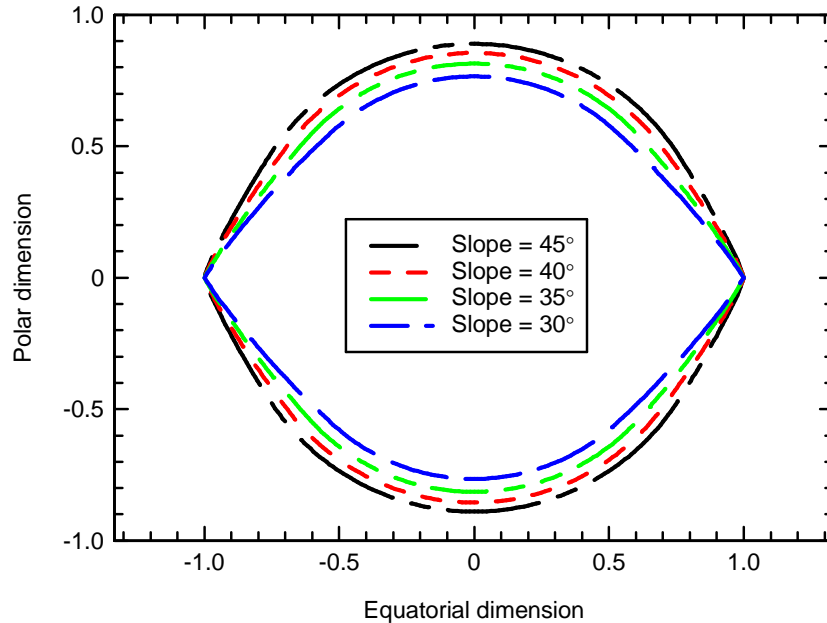


Figure 3. Figures of constant slope from the equator up to a latitude approximately equal to the complement of the critical slope angle, such that "landsliding" uphill is not permitted.

To fix this problem, we introduced a constraint in the program to hold the figure constant at latitudes greater than a specified value. As the figure adjusts from an initial shape (we chose a sphere for our main calculations), the polar dimension shrinks down and the equatorial dimension expands, and in the process the slope at higher latitudes decreases a bit, even if the shape of the "polar cap" is not changed. Thus we found that we had to tinker a bit with the latitude constraint in order to end up with figures that blended smoothly from constant slope at the chosen value of β to the decreasing slope at higher latitudes. Figure 3 is a set of figure profiles at equatorial aspect for a number of slope values spanning the range of typical "rubble" materials. These "nut-shaped" profiles look satisfyingly similar to the shape profile of (66391) 1999 KW4, as can be seen in Figure 4, comparing

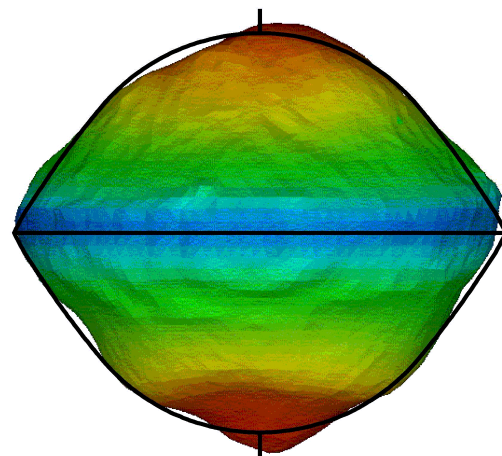


Figure 4. Constant-slope figure for critical slope of 37° compared to shape of (66391) 1999 KW4 (shape profile from Scheeres et al. 2006).

the actual shape to the slope = 37° model. It must be noted that due to smaller scale irregularities it is not possible to estimate the critical slope angle closer than around $\pm 5^\circ$.

3. Constant-slope shape of a non-spinning body

After experimenting a bit with the program, it occurred to us that the same program could be used to address the question of the maximum elongation of a non-spinning rubble pile body. If we imagine an extremely elongated "cigar-shaped" body, not spinning at all, the direction of local gravity at the surface will deviate from "vertical" by more than the allowed critical slope, and landsliding should occur, tending to collapse the body in the direction of a sphere. The question we ask is, how elongate can a body be and still not have slopes anywhere exceeding the critical slope angle? To investigate this, we can set $\delta = 1.0$, corresponding to zero centrifugal force, hence a non-spinning body, and start with an initial figure with "flattening" $f > 1$, corresponding to a body with polar dimension greater than the equatorial radius. This is of course perpendicular to the axis arrangement of a slowly spinning prolate ellipsoid, but does not matter since we are considering a body with no spin at all. Somewhat to our surprise, the program worked fine with values of $f > 1$, even though we had not coded it with that intention. Figure 5 is a plot of some results. We have rotated the figure 90° to correspond to a prolate body rotating slowly (not at all, in fact) about its short axis. We made a first run starting from a 5:1 elongate body, that is, with $f = 5$. In this case, it is the polar region that has slope greater than the critical value, so landsliding occurs from the long ends toward the "equator" (the short dimension), but does not extend down to the equator. We first calculated an unconstrained figure, starting from a 5:1 prolate ellipsoid, where the final equilibrium figure has a constant slope $\beta = 40^\circ$ everywhere, regardless of "landsliding uphill". A bi-lobed figure, which is analogous to the unconstrained shape in Figure 2 for a critically spinning body, resulted. We next constrained the shape not to change in the range (this time near the "equator") where slope was initially under the

critical value. The "torpedo" shaped figure is what results when we start from the same 5:1 prolate ellipsoid. Mass is not conserved in these calculations. Instead the equatorial (polar in this rotated view) dimension is held to a constant value of 1.0 in the calculation. In the figure, the unconstrained (bi-lobed) solution is rescaled to match the length of the constrained solution. In both solutions, the

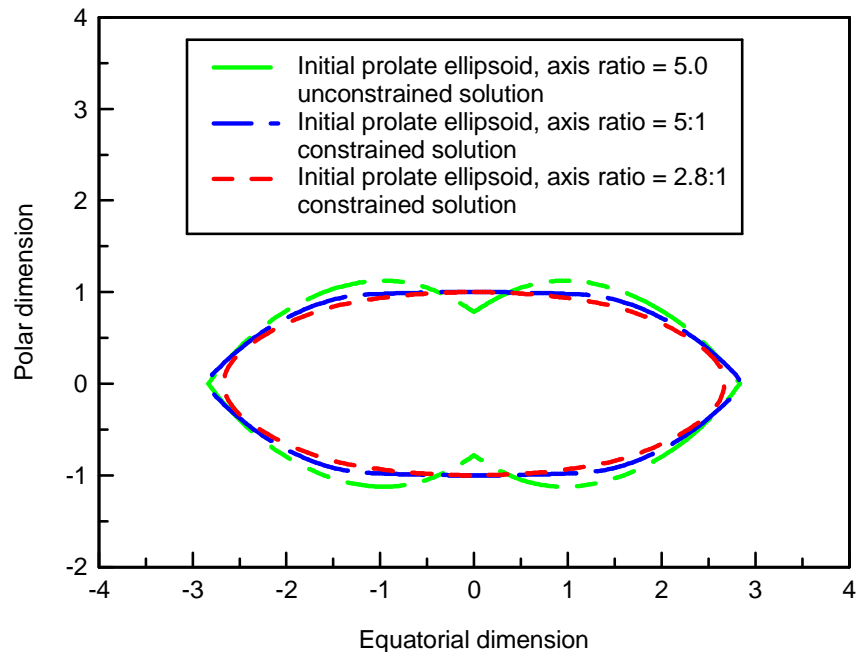


Figure 5. Constant-slope figures of prolate, non-rotating bodies. See text for complete description.

length to width ratio shrinks down to about 3:1. The odd shape of the bi-lobed solution appears a bit artificial, since we have constrained the "waist" of the figure to remain constant, yet matter must cascade down into that region from the long ends. Thus, the unconstrained bi-lobed shape is not as unphysical as the shape in figure 2, since some (maybe all) of the mass motion in the equatorial range is not "up hill". The bi-lobed shape is somewhat suggestive of some observed asteroid shapes, e.g. Toutatis, and may have some reality as the shape that results from slumping of an extremely elongate initial figure. Since our static model does not really give us much insight into dynamical mass motions, we looked at successively less elongate initial figures until we found the limit for a prolate ellipsoid that has no slope exceeding the critical value. For $\beta = 40^\circ$, this corresponded to a prolate ellipsoid with an axis ratio of 2.8:1. From the similarity of this figure to the other figures, we infer that the most extreme length-to-width figure that can be sustained by a rubble pile is in the range of about 3:1 axis ratio. This in fact is about what we see among the sampling of slowly rotating bodies, based on maximum lightcurve amplitudes, which typically don't much exceed about 1.2 magnitude among slowly rotating bodies, especially when corrected to zero phase angle to remove shadowing enhancement of the lightcurve amplitude. All three of the shapes in Figure 5 would have lightcurve amplitudes at zero phase and equatorial aspect of about one magnitude.

One further investigation we carried out with the program was to see how flat of an oblate spheroid could sustain its shape with $\beta < 40^\circ$. We started with $\delta = 1.0$, that is not rotation, and explored a range of $f < 1.0$ to see how flattened an oblate spheroid could sustain its shape as a rubble pile. We found that figures as flat as $f = 0.21$ (nearly 5 to 1 flattened) have surface slope everywhere under 40° and should not "landslide" toward a more spherical figure. Since we are here exploring a range of figures with symmetry about the stable spin axis, we can further investigate the stability of sub-critically, but non-zero, spinning bodies. For $\delta = 0.5$, that is with centrifugal force equal to half of gravity at the equator, slope remains everywhere under 40° for figures all the way down to $f = 0.10$, that is, an oblate spheroid with polar dimension only one tenth the equatorial dimension. We do not mean to suggest that such outrageously flattened figures exist in nature. The important point of this exercise is to note the extreme range of shapes that can exist among "rubble piles" without landsliding to more regular shapes. We infer from this that comparison of small asteroid shapes with "fluid equilibrium" shapes, and in particular inferring bulk densities of such bodies by comparison of actual shapes with fluid equilibrium shapes, is close to nonsense.

4. Tidal saltation on a critically spinning binary body

The asteroid (66391) 1999 KW4 is remarkable not only for its shape and constant slope profile, but even more so for the almost exact cancellation of gravitational and centrifugal accelerations at the equator. Indeed, the current spin of 1999 KW4 corresponds to about the value of $\delta = 0.01$ used in our calculations in Section 3. This seems too close to be coincidental, leading to the hypothesis that the primary of the system has been spun up over time, presumably by YORP torque, to the point of landsliding of material toward the equator, and then in some way shedding mass which re-accumulates in orbit to form a secondary. Perhaps even the growth of the secondary has been gradual over time as additional mass is shed. It is not the purpose of this paper to investigate the mechanism of mass shedding, but what we now direct attention to is the fact that in a close binary system, like 1999 KW4 and other small asynchronous binaries, the

gravitational acceleration on the primary is not constant, but in fact varies with the "diurnal" tide from the secondary. This variation, while small in magnitude, could in fact induce a major variation in the net acceleration vector along the equator, where the static component of gravity is already very nearly cancelled by centrifugal acceleration. Indeed, if the amplitude of the tidal acceleration were to be close to the factor δ of the constant gravitational acceleration, then a particle on the surface at the equator would feel the total acceleration vector go to zero as the satellite passed overhead. Any greater and it would become upward, resulting in the particle levitating off the surface. Our goal in this section is to explore this case and investigate the resulting particle motions near the equator, which we call "tidal saltation".

We consider only two-dimensional motion, in the equatorial plan of the primary, which is also assumed to be the plane of the orbit of the satellite. Let the rotational spin velocity to be ω and the orbit frequency be Ω . In a polar coordinate system (r, θ) centered at the CM of the primary and rotating with it (so a rock sitting still on the surface has constant coordinates), the equations of motion are:

$$\ddot{r} - r(\omega + \dot{\theta})^2 = -g + T_r, \quad (2)$$

$$r\ddot{\theta} + 2\dot{r}(\omega + \dot{\theta}) = T_\theta. \quad (3)$$

g is the gravitational acceleration from the primary, and T_r and T_θ are the tidal accelerations from the secondary, in the radial and tangential directions, respectively. Since the satellite is moving in this coordinate system, the tidal acceleration varies with a frequency of $(\omega - \Omega)$. The orbit frequency is:

$$\Omega = \sqrt{\frac{G(M+m)}{a^3}}, \quad (4)$$

where m is the mass of the satellite, and a is the orbit radius. The tidal accelerations are:

$$T_r = -\frac{Gm}{a^2} \left(\cos \alpha + \frac{r/a - \cos \alpha}{[1 + (r/a)^2 - 2(r/a) \cos \alpha]^{3/2}} \right), \quad (5)$$

$$T_\theta = \frac{Gm}{a^2} \sin \alpha \left(1 - \frac{1}{[1 + (r/a)^2 - 2(r/a) \cos \alpha]^{3/2}} \right), \quad (6)$$

where we have introduced the angle $\alpha = (\omega - \Omega)t + \theta$, which is the angle from overhead of the satellite at the time t . These equations reduce to the usual quadripole tidal expressions when $a \gg r$ (but note that the expressions in brackets reduce to zero to first order so that one must carry second-order terms to yield the usual $\cos(2\alpha)$ and $\sin(2\alpha)$ dependences. Even when a is not much greater than r (essentially, R), the tidal terms remain "diurnal" with extremes twice per "day". The above expressions are approximate in that we have assumed a spherical secondary figure rather than a triaxial ellipsoid one. However, expressions appropriate for a triaxial ellipsoid fit to the secondary of (66391) 1999 KW4 produce insignificant deviation in

results from the above much simpler approximate expressions. Figure 6 is a plot of the radial and tangential accelerations for $a/R = 3.33$, appropriate for (66391) 1999 KW4, on the equator and on the surface, $r = R$. Note that the tidal accelerations for this value of a/r , typical for asynchronous binaries, are about twice larger on the satellite side of the primary than on the back side. We will see that the onset of mass flow is so critically tuned to the magnitude of the tide that for such asynchronous binaries tidal saltation probably occurs only on the satellite-facing side of the primary.

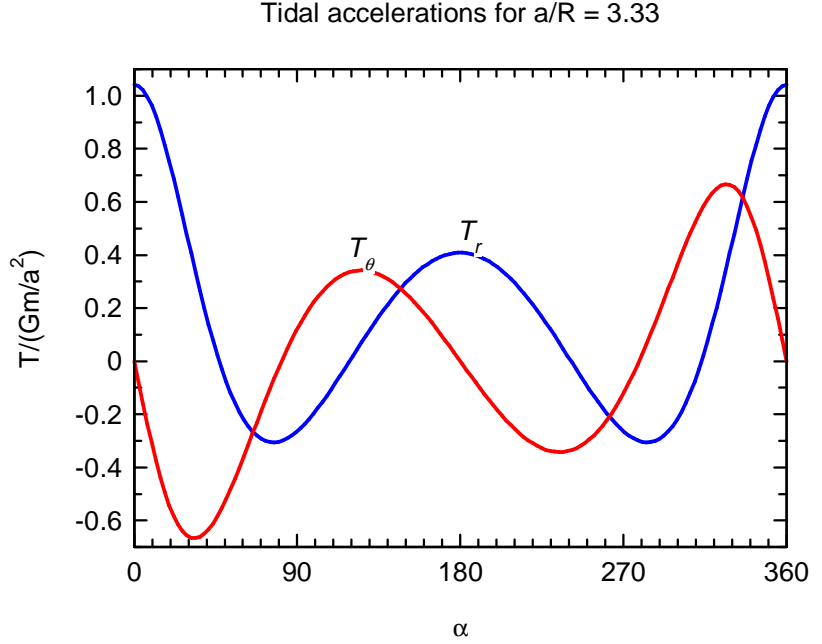


Figure 6. Radial and tangential tidal accelerations at the equator of the primary scaled appropriately for the separation of the (66391) 1999 KW4 binary.

We are interested in the case where $g \approx \omega^2 R$, so we make the substitution using δ as given in equation (1). However, for a particle which might levitate off the surface so that $r \neq R$, we need to account for the variation in g with r :

$$(1 - \delta)g = \omega^2 R \left(\frac{R}{r} \right)^2 \Rightarrow g \approx (1 + \delta)\omega^2 R \left(\frac{R}{r} \right)^2, \quad (7)$$

where it will be more convenient in what follows to use the right hand approximation, valid when $\delta \ll 1$. We further introduce another small quantity ε to replace the coefficients of the tidal accelerations in (5) and (6):

$$\varepsilon \omega^2 R = \frac{Gm}{a^2} \Rightarrow \varepsilon = \frac{m}{M + m} \frac{a}{R} \left(\frac{P_{rot}}{P_{orb}} \right)^2. \quad (8)$$

With this definition, when $\varepsilon = \delta$, the tidal acceleration on a stationary particle sitting on the equator directly under the satellite almost exactly cancels the differential acceleration (gravity minus centrifugal). Thus the range of interest to explore will be within a small range of $\varepsilon \approx \delta$. Our goal is to evaluate this motion over a range of values of δ and ε . As an example, we can evaluate values of δ and ε for the well-characterized binary asteroid (66391) 1999 KW4. Ostro et al. (2006) give values of $P_{orb} = 17.4223$ h; $P_{rot} = 2.7645$ h; $m = 0.135$ and $M = 2.353$ (10^{12} kg); and $a/R = 3.33$. These constants lead to a value of $\varepsilon = 0.00455$. δ is somewhat harder to evaluate, since the gravity field is irregular on the scale of δ . However, Scheeres et al. (2006)

state that "a rotation period only 1.3% shorter would place portions of Alpha's surface at orbital speeds." Thus, we can infer that $P_{rot}/P_{crit} \approx 1.013$, and thus $\delta \approx 0.026$. In the idealized case of a completely regular surface, the current tidal accelerations on (66391) 1999 KW4 are insufficient to result in mass levitation, but local irregularities might lead to some motions even presently.

Equations (2) and (3) can now be written in terms of the small quantities we have defined:

$$\ddot{r} - r(\omega + \dot{\theta})^2 = -(1 + \delta)\omega^2 R \left(\frac{R}{r} \right)^2 - \varepsilon\omega^2 R \left(\cos \alpha + \frac{r/a - \cos \alpha}{[1 + (r/a)^2 - 2(r/a) \cos \alpha]^{3/2}} \right), \quad (9)$$

$$r\ddot{\theta} + 2\dot{r}(\omega + \dot{\theta}) = \varepsilon\omega^2 R \sin \alpha \left(1 - \frac{1}{[1 + (r/a)^2 - 2(r/a) \cos \alpha]^{3/2}} \right). \quad (10)$$

The equations become somewhat simpler for the case of motion (or no motion) confined to the surface of the body, where $r = R$:

$$\ddot{r} = R(\omega + \dot{\theta})^2 - (1 + \delta)\omega^2 R - \varepsilon\omega^2 R \left(\cos \alpha + \frac{R/a - \cos \alpha}{[1 + (R/a)^2 - 2(R/a) \cos \alpha]^{3/2}} \right), \quad (11)$$

$$R\ddot{\theta} = \varepsilon\omega^2 R \sin \alpha \left(1 - \frac{1}{[1 + (R/a)^2 - 2(R/a) \cos \alpha]^{3/2}} \right). \quad (12)$$

The above equations are valid as long as the test mass is on the surface, and the acceleration vector, \ddot{r} , is negative, that is with a net acceleration downward. In such a case, of course, the actual radial acceleration of the particle is resisted by the surface of the primary and is zero. But equation (11) remains the critical test for levitation: as long as $\ddot{r} \leq 0$, the motion is confined to the surface. Once the particle levitates, then \ddot{r} can (and will) become less than zero. The critical test then for free flight is whether $r > R$. Thus, equations (9) and (10) govern the motion of the test particle in flight; equations (11) and (12) govern sliding motion on the surface. Equation (11) can be further simplified for the static case, where the test particle is not even sliding. In such a case $\dot{\theta}$ is also zero, so the first two terms on the right reduce to $-\delta\omega^2 R$:

$$\ddot{r} = -\delta\omega^2 R - \varepsilon\omega^2 R \left(\cos \alpha + \frac{R/a - \cos \alpha}{[1 + (R/a)^2 - 2(R/a) \cos \alpha]^{3/2}} \right). \quad (13)$$

This simplified form of (11), combined with (12), can be used to determine whether the tangential acceleration is great enough to trigger sliding motion:

$$R|\ddot{\theta}| > -\ddot{r}\mu_s, \quad (14)$$

where μ_s is the coefficient of static friction. This relation is simply the definition of μ_s , but provides the recipe for testing for the onset of sliding motion in terms of the radial and tangential forces \ddot{r} and $R\ddot{\theta}$. In determining if mass motion occurs, this relation only makes sense, of

course, if \ddot{r} is less than zero, that is, pointing down. Here we are considering the case of a level surface subject to an acceleration vector that deviates from vertical. This is exactly analogous to considering a sloping surface with respect to a vertical acceleration vector, as exists for example, for a sloping field of loose rubble formed by a landslide. The condition for stability against landsliding is often stated in terms of the maximum slope that a material such as sand, loose rock, or whatever can withstand before landsliding occurs. This angle is sometimes called the *angle of slide*, $\tan \beta_s = \mu_s$. A similar angle, the *angle of repose*, β_r , is the slope at which a landslide stops, or comes to rest. This angle is related to the coefficient of sliding (kinetic) friction, $\tan \beta_r = \mu_k$, which we will use in the equation of sliding motion. For typical dry rubble on the Earth, the angle of repose is around 35° . The angle of slide is typically 5° to 10° greater. Thus, we will take as nominal values $\beta_r = 35^\circ$ and $\beta_s = 42^\circ$, corresponding to $\mu_k = 0.7$ and $\mu_s = 0.9$, although we retain them as parameters that can be set to different values. The picture that is on the cover of the issue of *Science* with the Ostro *et al.* and Scheeres *et al.* papers in it is in fact a map of exactly this slope of the surface of the asteroid 1999 KW4 with respect to the local acceleration vector. The fact that almost the entire surface is a uniform green, corresponding to a slope in the $35\text{-}40^\circ$ range indicates that (a) the surface is in a sort of "landslide equilibrium", just short of further mass motion, and (b) an angle of repose around 35° is apparently about right for the material composing 1999 KW4.

One further set of equations is needed, to describe the "landslide" state of motion, where the condition (14) is met or $\dot{\theta} \neq 0$, but $\ddot{r} < 0$ and $r = R$, thus the test mass is on the surface, but should begin (or continue) sliding. Once sliding motion is initiated, μ_s is not relevant; the test mass continues sliding until either \ddot{r} becomes positive and the mass levitates into free flight, or if it is decelerating until it skids to a halt. The usual formulation for sliding motion is to parameterize the resisting force (acceleration) in terms of a coefficient of kinetic friction, μ_k . The resisting force in the tangential direction is μ_k times the "weight" of the object, thus the retarding force (acceleration) on the mass is just equal to $\mu_k \ddot{r}$, in the tangential direction opposing $\dot{\theta}$. Thus we have:

$$R\ddot{\theta} = \varepsilon\omega^2 R \sin \alpha \left(1 - \frac{1}{[1 + (R/a)^2 - 2(R/a) \cos \alpha]^{3/2}} \right) + \mu_k \ddot{r} \frac{\dot{\theta}}{|\dot{\theta}|}. \quad (15)$$

Keep in mind that \ddot{r} is a negative quantity, so the second term is in a direction opposing $\dot{\theta}$. μ_k is always less than μ_s . That is, resistance is less once sliding begins, as anyone who has driven a car in a skid knows.

We now have collected all the necessary equations to describe the mass motion, if any, of material along the equator of an asynchronous binary. For chosen values of δ , ε , μ_s and μ_k , one can test for a given value of α using (14) to determine if a particle is stable against any sliding motion. For $\mu_k = 0.9$ and the current values of δ and ε , 1999 KW4 is stable against mass motion for any value of α . However, a very slight change in spin period due to YORP acceleration could change that. Following the onset of sliding motion, equation (15) applies to track the tangential position and velocity. Equation (11), using the integrated value of $\dot{\theta}$, must be monitored to determine if levitation occurs ($\ddot{r} > 0$). If this occurs, then equations (9) and (10) apply, which can be integrated for free flight motion as long as $r > R$. When the test mass falls

back to the surface, we assume the vertical velocity, \dot{r} , is immediately damped to zero, but the tangential velocity, $R\dot{\theta}$, continues, and the sliding motion equation (15) is used to continue following the motion. When $R\dot{\theta}$ reaches zero, motion stops and the integration is over.

Figure 7 is a plot of the motion of a particle, starting out from rest on the equator of a sphere spinning at close to the critical rate, with values of $\delta \approx 0.005$. This range was chosen because the resulting differential acceleration at the equator (gravity minus

centrifugal), δg , is in the range of the current maximum radial tidal acceleration, T_{\max} (at $\alpha = 0$, from eq. 5 and Fig. 6) for 1999 KW4. What determines the nature of the motion (or lack thereof) of a particle is the ratio of the maximum tidal acceleration to the differential acceleration, $T_{\max}/\delta g$. This ratio is proportional to ε/δ , and for the constants we have used for 1999 KW4, are almost equal, that is, $T_{\max}/\delta g = 1.0$ corresponds to $\varepsilon/\delta = 0.96$. In Fig. 7 we plot trajectories for $T_{\max}/\delta g = 0.9, 1.0$, and 1.1 , in each case holding $\varepsilon = 0.00455$, and adjusting δ to obtain the listed value of $T_{\max}/\delta g$. This calculation was done for $R = 0.75$ km (the equatorial radius of 1999 KW4), but we found that the linear motion scales linearly with R , all other constants being the same. That is, on an asteroid with 1.5 km radius, the motions would be twice as large for the same value of $T_{\max}/\delta g$. Recall that for $T_{\max}/\delta g < 1.0$, a static particle would remain on the surface. We found, however, at a value of $T_{\max}/\delta g$ as low as 0.76 the test particle would begin to slide on the surface in the direction of the tidal force. Remarkably, almost as soon as the onset of sliding motion, the added velocity of the particle along the surface would result in an increase in centrifugal force enough to result in levitation of the particle and a period of free flight before falling back to

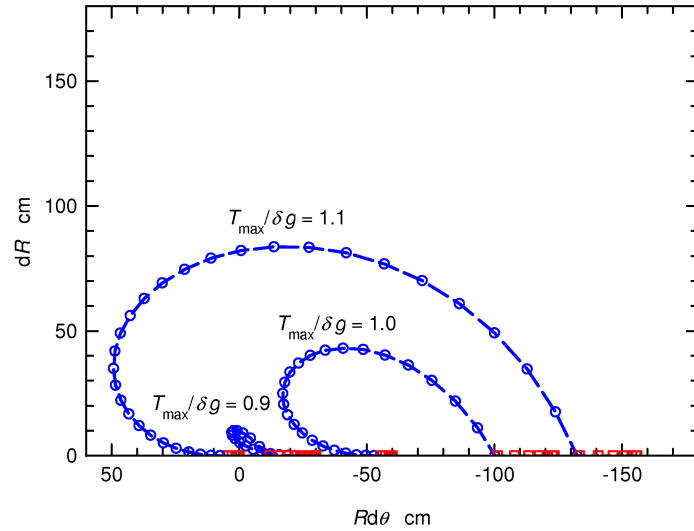


Figure 7. Motion of a particle on the equator of a near-critically spinning sphere. See text for description.

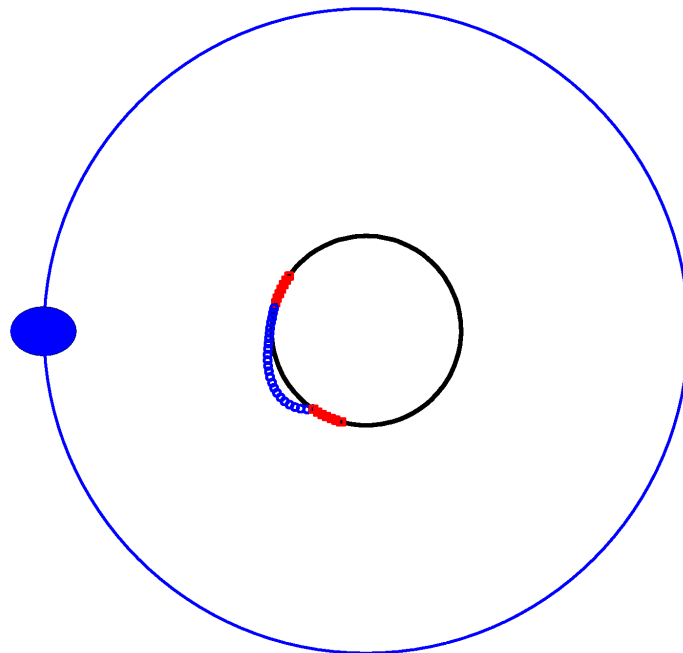


Figure 8. Motion as seen in coordinates rotating with the satellite. Radial height exaggerated 300 times. Only the path for $T_{\max}/\delta g = 1.0$ is shown.

the surface. So even with a value of $T_{\max}/\delta g = 0.84$ there is a small period of free flight, and for $T_{\max}/\delta g = 1.0$ it is a quite substantial “hop”. In the figure, the satellite rises from the left, moves overhead, and sets to the right. Motion begins with sliding motion toward the left (red box symbols), followed by levitation into free flight (blue circles) rising up and moving back toward the right, then falling back to the surface to the right (behind except for the case of very limited motion) where the particle started out (more red boxes). The scale here is in units of 10^{-5} radii of the body, thus for a 1 km radius body, the scale would be in centimeters. Thus, for $T_{\max}/\delta g = 1.0$, a particle would levitate 6 cm or so above the surface and land back 10 cm or so behind where it started. For $T_{\max}/\delta g = 0.9$, the levitation would be only a centimeter or two, and that particle would come to rest very close to where it started. For $T_{\max}/\delta g = 1.1$, the scale of the motion is more than twice greater than for $T_{\max}/\delta g = 1.0$, so it is clear that the onset of motion is very sharp with increasing tidal strength (or decreasing spin-gravity differential).

Figure 8 is a plot of the same particle motions, but in polar coordinates rotating with the satellite. So in this view, the satellite is always to the left, as shown, and the primary is rotating counterclockwise below it. In order to show the radial levitation at all, we have exaggerated the radial scale of the particle above the surface by a factor of 300. Only one path is shown, for $T_{\max}/\delta g = 1.0$, for clarity. As expected, the onset of motion is near the maximum tangential tidal acceleration, around 45° before the satellite passes overhead. But the end of motion continues to about 90° after the satellite passes overhead, and in fact the interval of levitated motion peaks well past the overhead point. This results in a geometry exactly like a tidal lag, with the result that there should be a torque transferring angular momentum from the primary spin to the satellite orbit, exactly as results from tidal friction. But in this case, the tidal lag angle is much larger than for a solid body tide, and the scale of motion (centimeters for a km-size body) is much larger than tidal flexing of such a small elastic body. However, the mass involved in this motion may be much less than the whole mass of the primary, so the actual rate of torque transfer will depend critically on the amount of mass involved in this motion.

It is important to note, however, that unlike tidal friction, which is nearly independent of the spin rate of the primary, this process is very sharply dependent on spin rate, and in fact shuts off entirely at only a little under the critical spin rate. Thus, if tidal friction were the dominant torque present, we would expect the primary to spin down as angular momentum were transferred to the secondary. In contrast, the “tidal saltation” process works effectively only very near the critical spin, so if YORP is also acting to spin the primary up, tidal saltation serves only to “put the brakes on” very close to the spin limit, but does not slow it down much below the critical rate.

We can evaluate the energy loss per unit mass in motion, which could then be used to estimate the torque transfer. The sliding energy loss is just the resisting force, $\mu_k \dot{r}$, integrated over distance, $Rd\theta$, thus $\Delta E / \Delta M = \int |\mu_k \dot{r} R d\theta|$ over the range of θ of the sliding motion, both before and after any period of levitation. In free flight, energy is conserved, but on impact, the energy associated with the vertical component of motion, $\dot{r}_{imp}^2 / 2$, is lost. Thus the total energy lost per cycle is:

$$\frac{\Delta E}{\Delta M} = \int |\mu_k \dot{r} R d\theta| + \frac{1}{2} \dot{r}_{imp}^2 \quad (16)$$

By tracking the energy lost per cycle we can evaluate the equivalent of "tidal friction" leading to the slowing of the spin of the primary and the expansion of the orbit of the satellite. The tricky part is estimating the amount of mass ΔM that participates in the motion. We have not attempted to do this, as one would need a proper hydrocode integrator with suitable equations of state to describe the motions of particles under the surface, rather than just a simple "sliding particle on the surface" model. It seems apparent to us, however, that the process we show here is very sensitive to the quantity ε/δ , so if a slow process like YORP is continuously adding angular momentum, thus increasing the value of ε/δ , the onset of mass motion on the surface will start transferring the accumulating angular momentum so that a quasi-equilibrium will be established at whatever value of ε/δ results in transferring momentum at the rate it is received by YORP.

Conclusion

Obviously, this is an unfinished work. The shape and landsliding study uses a purely static model. We do not attempt to realistically model the dynamical process of mass motion once a "landslide" is initiated. On a nearly critically spinning body a "landslide" toward the equator would no doubt take on a cyclonic sort of motion due to the coriolis force. Whether such a landslide would result in a discrete fission event to form a satellite or a slow mass shedding is beyond our simple algorithm to determine. Likewise, our simple model of sliding friction on the surface and levitation into free flight (orbital) motion provides a "cartoon" of a process, which we have called "tidal saltation", that we suspect serves to transfer angular momentum from primary spin to satellite orbit, analogous to the process of tidal friction. This process appears to be capable of regulating the gain of angular momentum by a satellite system by YORP effect, and hold the primary near the critical spin limit.

But what happens next? After the satellite recedes a certain distance, the tidal interaction will become too weak to levitate mass off the surface. Perhaps at this point the primary will over-spin, experience more landsliding, and create another satellite, by mass shedding or fissioning. Two very recent discoveries bear on this matter. One is the discovery of a regular system of two satellites about the NEA 2001 SN263 (Nolan et al. 2008). Perhaps what we see here is one satellite that has receded too far to be effective in controlling the continuing gain of angular momentum, so the primary overspins and creates another inner satellite. The other fascinating discovery is a significant number of pairs of asteroids in extremely similar heliocentric orbits, suggesting a common origin from a single, or binary, body in the last few tens of thousands of years (Vokrouhlicky and Nesvorny 2008). It appears that these may be "divorced" binaries that have come apart by gravitational processes such as described by Scheeres (2007). The fact that we actually see multiple examples with such short lifetimes suggests that binary formation and evolution among small asteroids is a very dynamic process and that most systems we currently see are very young.

References

Chandrasekhar, S. (1969) *Ellipsoidal Figures of Equilibrium*. New Haven and London: Yale University Press, 253pp.

- Holsapple, K. A. (2004) Equilibrium figures of spinning bodies with self-gravity. *Icarus* **172**, 272–303.
- Nolan, M. C., E. S. Howell, L. A. M. Benner, S. J. Ostro, J. D. Giorgini, M. W. Busch, L. M. Carter, R. F. Anderson, C. Magri, D. B. Campbell, J. L. Margot, R. J. Vervack, Jr., and M. K. Shepard (2008) (153591) 2001 SN₂₆₃. IAU Circular No. 8921.
- Ostro, S. J., J.-L. Margot, L. A. M. Benner, J. D. Giorgini, D. J. Scheeres, E. G. Fahnestock, S. B. Broschart, J. Bellerose, M. C. Nolan, C. Magri, P. Pravec, P. Scheirich, R. Rose, R. F. Jurgens, E. M. De Jong, and S. Suzuki (2006) Radar imaging of binary near-Earth asteroid (66391) 1999 KW₄. *Science* **314**, 1276-1280.
- Scheeres, D. J., E. G. Fahnestock, Ostro, S. J., J.-L. Margot, L. A. M. Benner, S. B. Broschart, J. Bellerose, J. D. Giorgini, M. C. Nolan, C. Magri, P. Pravec, P. Scheirich, R. Rose, R. F. Jurgens, E. M. De Jong, and S. Suzuki (2006) Dynamical configuration of binary near-Earth asteroid (66391) 1999 KW₄. *Science* **314**, 1280-1283.
- Scheeres, D. J. (2007) Rotational fission of contact binary asteroids. *Icarus* **189**, 370-385.
- Shepard, M. K., J.-L. Margot, C. Magri, M. C. Nolan, J. Schlieder, B. Estes, S. J. Bus, E. L. Volquardsen, A. S. Rivkin, L. A. M. Benner, J. D. Giorgini, S. J. Ostro, M. W. Busch (2006) Radar and infrared observations of binary near-Earth Asteroid 2002 CE₂₆. *Icarus* **184**, 198-210.
- Vokrouhlicky, D. and D. Nesvorny (2008) Pairs of asteroids probably of common origin. Subm. to *Astron. J.*